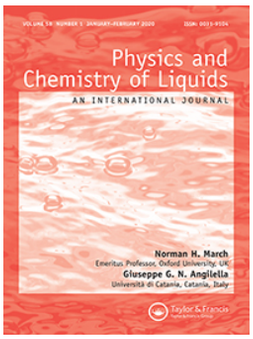

Taylor & Francis
Taylor & Francis Group

Physics and Chemistry of Liquids

An International Journal

ISSN: 0031-9104 (Print) 1029-0451 (Online) Journal homepage: www.tandfonline.com/journals/gpch20

Conformational, spectroscopic, optical, physicochemical and molecular docking study of 4-methoxy-benzaldehyde oxime and 4-hydroxy-3-methoxy-benzaldehyde oxime

Yunus Kaya, Ilhan Kucuk & Asli A. Kaya

To cite this article: Yunus Kaya, Ilhan Kucuk & Asli A. Kaya (2020) Conformational, spectroscopic, optical, physicochemical and molecular docking study of 4-methoxy-benzaldehyde oxime and 4-hydroxy-3-methoxy-benzaldehyde oxime, Physics and Chemistry of Liquids, 58:1, 77-93, DOI: 10.1080/00319104.2018.1550775

To link to this article: https://doi.org/10.1080/00319104.2018.1550775

PHYSICS AND CHEMISTRY OF LIQUIDS
2020, VOL. 58, NO. 1, 77–93
https://doi.org/10.1080/00319104.2018.1550775

Taylor & Francis
Taylor & Francis Group

ARTICLE

Conformational, spectroscopic, optical, physicochemical and molecular docking study of 4-methoxy-benzaldehyde oxime and 4-hydroxy-3-methoxy-benzaldehyde oxime

Yunus Kaya[a], Ilhan Kucuk[a] and Asli A. Kaya[b]

[a]Faculty of Engineering and Natural Sciences, Department of Chemistry, Bursa Tech University, Bursa, Turkey; [b]Faculty of Arts and Sciences, Dept. Physics, Bilecik Seyh Edebali Univ, Bilecik, Turkey

ABSTRACT

In this study, the conformational, spectroscopic, optical, physicochemical and molecular docking studies of two oxime molecules, namely 4-methoxy-benzaldehyde oxime (mboH) and 4-hydroxy-3-methoxy-benzaldehyde oxime (hmboH) were reported. The conformational analyses and spectroscopic properties were performed by DFT/B3LYP method and 6–311++G(d, p) basis set to find the most probable geometries of both molecules. The optical properties, energy gap and nonlinear optical (NLO) properties were investigated in different solvents which are benzene, chloroform, ethanol, dimethyl sulfoxide (DMSO) and water. Some physicochemical properties were also performed. The stability of the mboH and hmboH arising from hyper-conjugative interaction and charge delocalisation has been analysed using natural bond orbital (NBO) analysis. The stability of the molecules arising from hyper conjugative interactions and charge delocalisation has been also analysed using NBO study. In addition, molecular docking studies with DNA and protein structures to find the most preferred binding mode of the ligands inside the DNA and protein cavity.

ARTICLE HISTORY
Received 17 August 2018
Accepted 18 November 2018

KEYWORDS
Oxime; DFT calculation; spectroscopic properties; optical properties; nonlinear optics; molecular docking

1. Introduction

Oxime molecules as a structure played a significant role in the theoretical chemistry [1–5]. Since the oxime group possesses two heteroatoms such as the nitrogen and oxygen atoms, these molecules show interesting electronic future. These type molecules are also synthesised by experimentalists due to their potential coordination behaviour [6–8]. Generally, the coordination occurs via the nitrogen atom. In addition, these type molecules, structures and electronic properties are important as theoretically or experimentally, due to the fact that they showed versatile antimicrobial activity [9–11] and they exhibited high DNA binding affinity as well as significant cytotoxic activity [12–15].

With the development of computer science in recent years, many important chemical and physical properties of chemical systems can be obtained by various calculation techniques [16]. The most popular of these techniques for calculations in theoretical modelling is density functional theory (DFT). In many cases, the results of DFT calculations for solid state systems agreed quite satisfactorily with the experimental data. DFT predicts a great variety of molecular properties; geometry, conformational analysis, vibrational frequencies, absorption and emission spectra, NMR spectra, ionisation energy, magnetic properties, atomic charges, thermodynamic features,

CONTACT Asli A. Kaya asli.kaya@bilecik.edu.tr Faculty of Engineering and Natural Sciences, Department of Chemistry, Bursa Tech University, Bursa, Turkey

Supplementary material for this article can be accessed here.

reaction paths, etc. The theoretical studies on isomerisations, reaction mechanisms and spectroscopic properties of some oximes were performed in the literature [1,17–27]. As far as we have examined, the molecular structures of the mboH and hmboH, experimental and theoretical spectroscopic properties and some physicochemical properties have not been presented yet in the literature. Therefore, in this study, the synthesis, characterisation and spectroscopic properties (IR and UV-vis) were reported as experimentally. In addition, DFT calculations were performed to explain the structures, spectroscopic properties (IR and UV-vis) and some physicochemical properties, such as the nonlinear optical (NLO) properties, the molecular electrostatic potential (MEP), the Frontier molecular orbitals (FMOs), energy gap between HOMO and LUMO orbitals, atomic charges, Fukui function indices, the first hyperpolarisibility, the natural bond orbital (NBO) analysis and thermodynamic properties with different temperatures. The molecular docking studies were performed with Autodock/vina to explain the interaction of mboH and hmboH with DNA and HSA, since the oxime molecules can be potential antimicrobial activity. These calculations are precious for providing insight into molecular properties of oxime compounds.

2. Materials and methods

2.1. *Instrumentation*

All chemicals used in the experiments were purchased commercially and used without further purification. The elemental analyses for C, H and N were performed using a EuroEA 3000 CHNS elemental analyser. UV-vis spectra were measured on an Agilent Cary60 spectrophotometer. IR spectra were recorded on a Perkin Elmer Spectrum Two FT-IR spectrophotometer.

2.2. *Synthesis*

The mboH and hmboH were synthesised according to the literature [28]. The mboH and hmboH were prepared by refluxing a mixture of a solution containing respective aldehyde (0.680 g, 4-methoxy-benzaldehyde; 0.761 g, 4-hydroxy-3-methoxy-benzaldehyde; 5 mmol) and 0.400 g NaOH (5 mmol) are mixed in a flask. 0.348 g hydroxylamine hydrochloride are added in small portions at a time, the reaction mixture was stirred for 4 h under reflux. The reaction temperature rose 80 °C. On cooling, a crystalline mass separates out. These reactions are illustrated in Scheme S1.

mboH: Colour, white. [Yield: 0.722 g, 96%]. M_w: 151.16 g.mol^{-1}. Anal. Found: C, 63.38; H, 5.88; N, 9.31% Calc: C, 63.56; H, 6.00; N, 9.27%. IR(ATR, cm^{-1}): νOH 3320 br, νCH 3009 w, 2976 w, 2940 w, 2842 w, νCN 1627 w, νCC 1608 m, 1576 m, δOH 1418 m, νNO 964 s.

hmboH: Colour, white. [Yield: 0.774 g, 93%] M_w: 167.16 g.mol^{-1} Anal. Found: C, 57.32; H, 5.12; N, 8.44% Calc: C, 57.48; H, 5.43; N, 8.38%. IR(ATR, cm^{-1}): νOH 3444 br, νCH 3011 w, 2945 w, 2867 w, νCN 1647 w, νCC 1599 m, δOH 1430 s, νNO 948 s.

2.3. *Computational details*

All quantum chemical calculations in this work were carried out using Gaussian 09 software packed [29]. The energy minimization was carried out for the oxime, methoxy and hydroxy groups for both molecules. The most stable conformation of the mboH and hmboH were calculated using DFT with dispersion correction were estimated using the wB97X-D/6–311++G (d,p) level developed by Grimme and co-workers [30] changing and scanning the dihedral angles C2-C1-C7-N1 and C3-C4-O2-C8 for mboH and the dihedral angles C2-C1-C7-N1, C2-C3-O3-C8 and C3-C4-O2-H for hbmoH. The structures of mboH and hmboH were reoptimized at the Becke–Lee–Yang–Parr functional (B3LYP) method [31] with 6–311++G(d,p) basis set. Harmonic frequencies of the both molecules were calculated at the same method and basis set to find local

minima, and all calculated frequencies are positive. The optimised structural parameters were used for all of the spectroscopic, molecular docking and physicochemical calculations, such as FMOs, MEP map, energy gap between HOMO and LUMO orbitals, the NBO analysis, thermodynamic and NLO properties in this study.

The harmonic vibrational frequencies obtained calculations were scaled by 0.958 [32] for 4000–1700 cm^{-1} and 0.978 [33] for 1700–400 cm^{-1} ranges, respectively. Vibrational band assignments were made using the GaussView molecular visualization program [34]. Transition energies and oscillator strengths for electronic excitation to the first 12 singlet-to-singlet excited states of the title compounds were calculated using TDDFT with the CAM-B3LYP/6–311++G(d,p) level. In addition, electronic absorption spectra were calculated in EtOH solution using the CPCM method.

In order to the detailed information about reactivities of mboH and hmboH, chemical reactivity parameters, chemical hardness (η) [35], chemical potential (μ) [35], and electrophilicity index (ω) [36] were evaluated from HOMO and LUMO energies. On the other hand, dipole moment is a useful index for the description of interactions between two chemical species. Therefore, the larger the dipole moment is, the stronger the van der Waals interaction will be. The chemical hardness (η) and the chemical potential (μ) are fundamental indicators of the stability and overall reactivity of a chemical system. The electrophilicity index (ω) allows quantitative description of the global electrophilic or nucleophilic nature of chemical species, physically signifying the propensity of chemical species to accept electrons.

2.4. *Molecular docking*

Molecular docking studies were performed using Autodock/Vina program [37]. The PDB formats of the mboH and hmboH were obtained by converting their out files using Autodock software. The crystal structures of B-DNA (PDB ID: 1BNA) and HSA (PDB ID: 5FCT) were retrieved from the Protein Data Bank. Visualisation of the docked systems was performed using Discovery Studio 3.5 software. The binding sites were centred on the DNA and HSA, and a grid box was created with 60 × 60 × 60 points and a 0.375 Å grid spacing in which almost the entire macromolecules were involved. All other parameters were kept at their default values.

3. Results and discussion

The discussions of synthesis and characterisation were presented in Supplementary materials (Figure S1).

3.1. *Conformational analysis and optimised structures*

In calculations firstly the potential energy surface (PES) of the compounds were scanned around the dihedral angles C2-C1-C7-N1 and C3-C4-O2-C8 for mboH and the dihedral anles C2-C1-C7-N1, C2-C3-O3-C8 and C3-C4-O2-H for hbmoH from 0 to 180° at increments of 10° at wB97X-D/6–311++G(d,p) level. The PES showed one minimum energy structure for both molecules as seen in Figure 1. The corresponding dihedral angles in most stable conformers for the mboH and hmboH molecules were calculated as ω1 = ω2 = 0° and ω1 = ω2 = 180°, ω3 = 0°, respectively. These results clearly indicate that the molecular structures of the title compounds are planar except methyl group, belongs to C_s point group symmetry as seen in Figure 2.

The molecular structures of mboH and hmboH were optimised by the DFT and B3LYP method with 6–311++G(d,p) basis set. The bond lengths, bond angles and dihedral angles of the mboH and hmboH molecules are listed in Table S1, while the optimised structures with numbering of atoms are shown in Figure 2. The mboH and hmboH molecules consist of 20 and 21 atoms, respectively. These molecules have six CC bonds, one CN bond and one NO bond. In

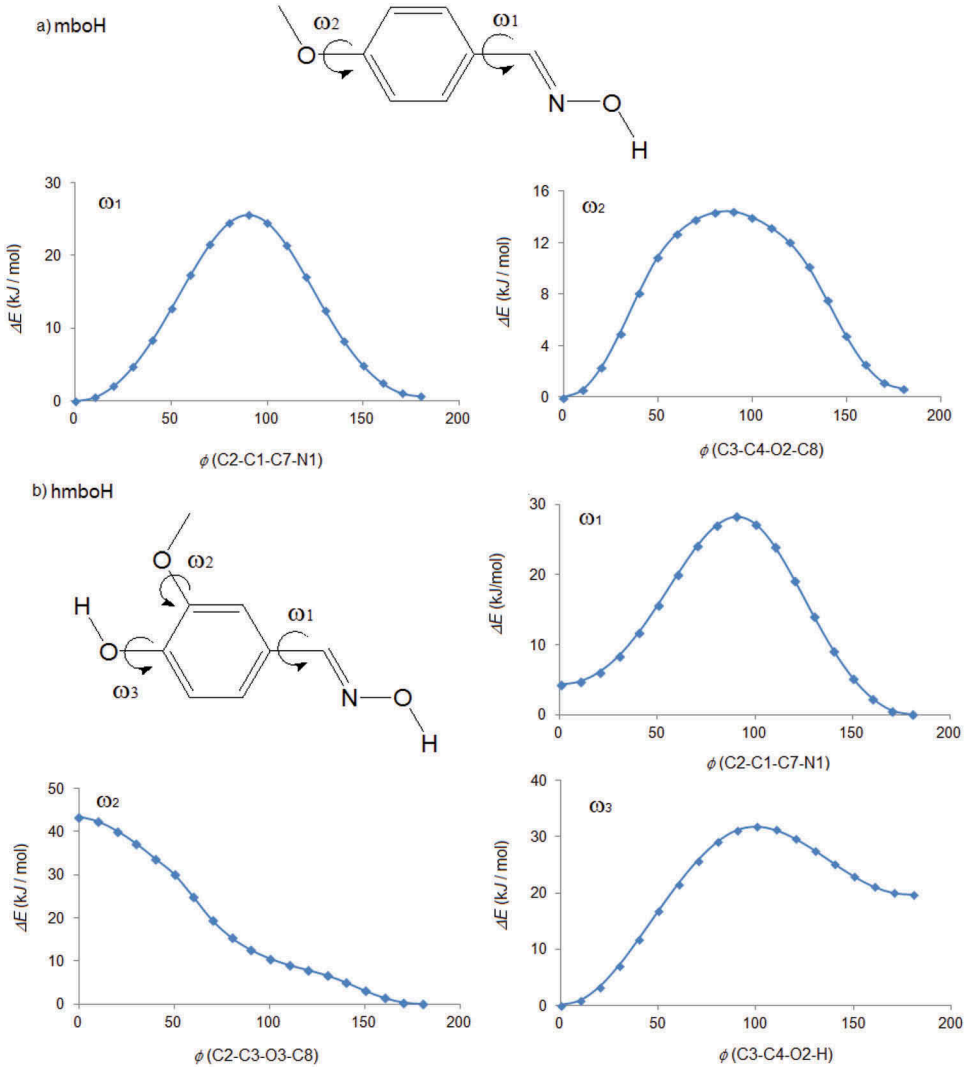

Figure 1. Potential energy surfaces of a) mboH for rotation ω1, ω2 and b) hmboH for rotation ω1, ω2, ω3 calculated at level of wB97X-D/6–311++G(d,p).

addition, the mboH has two CO bonds and one OH bond, while the hmboH has three CO bonds and two OH bonds. Generally, the molecular geometry is calculated in the gas phase, so the geometrical parameters may differ from the solid state, owing to the extended hydrogen bonding and stacking interactions. The average bond distances of CC bond of phenyl rings of mboH and hmboH molecules calculated by DFT/B3LYP method with 6–311++G(d,p) basis set are 1.396 and 1.393 Å, respectively. The CN double bond and NO single bond of oxime group of both molecules were calculated at 1.277 and 1.384 Å, respectively. These bond lengths agree well with the reported results on the oximes [5,38,39]. In the phenyl ring, the σ bond occurs between carbon and hydrogen atoms. A large attraction is exerted on the valence electron cloud of the hydrogen atom by the ring carbon atoms resulting in an increase in the CH force constant and in turn a decrease in the bond length in substitution benzenes. The CH bond lengths were calculated to have an average of 1.073 Å in the both molecules. The bond length OH shows a comparatively smaller value (0.974 Å for both molecules). In these molecules, the bond angle C7-N1-O1 116.5°

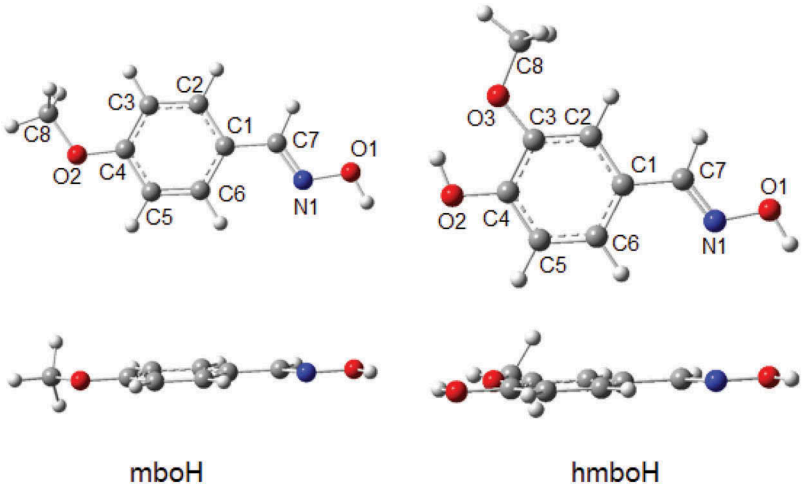

Figure 2. Optimized structures and atomic numbers of the mboH and hmboH.

for both molecules. The C8-O2-C4 bond angle was calculated at 118.8° in the mboH, while the bond angle C8-O3-C3 is 118.7° in the hmboH. Some selected dihedral angles are listed in Table S1. The planarity of the mboH and hmboH can be understood on the angle values to be 0° and 180°.

3.2. *Spectroscopic properties*

3.2.1. *Vibrational spectra*

The mboH and hmboH molecules containing N number of atoms have maximum number of potentially active observable fundamentals given by 3N-6. The title molecules, mboH and hmboH consist of 20 and 21 atoms, i.e. 54 and 57 normal vibrational modes. The calculated frequencies with the intensity less than 10 were not taken into consideration. The vibrational frequencies obtained for the title compounds with the unscaled B3LYP/6–311++G(d,p) force field is detected to be slightly greater than the experimental values. The calculated frequency values generally scaled for comparison of experimental and calculated values, due to improve the agreement between the predicted and observed frequencies and to compensate for the errors arising from the basis set incompleteness and to neglect of vibrational anharmonicity. The vibrational frequencies are scaled to 0.958 (above 1700 cm^{-1}) and 0.978 (below 1700 cm^{-1}) for B3LYP/6–311++G(d,p) level. The resultant scaled frequencies and measured infrared are presented in Tables S2 and S3, while comparative representations of experimentally and theoretically IR spectra of mboH and hmboH are given in Figure 3. The band centred at 3320 cm^{-1} for mboH and 3444 cm^{-1} for hmboH correspond to the vibration of the hydroxyl group. These stretching vibrations were calculated at 3472 and 3617 cm^{-1}, respectively. The deviation between the experimental and calculated values seems to be significant for the hydroxyl groups frequencies with a difference of 152 and 173 cm^{-1}, since IR vibration frequencies are calculated anharmonically [40]. The calculated aromatic and aliphatic CH vibrations were found in the range of 3027–2878 cm^{-1}, in agreement with the experimental values. The experimental CN bands of oxime group for mboH and hmboH were observed at 1627 and 1647 cm^{-1} respectively as weak bands and the calculated values of this mod were at ca 1633 cm^{-1} for both molecules. In the IR spectra of mboH and hmboH, there have been observed two CC vibration bands in both molecules, which are at 1608 and 1576 cm^{-1} for mboH and 1599 and 1517 cm^{-1} for hmboH. These bands were calculated at 1613 and 1569 cm^{-1} for mboH, 1609 and 1514 cm^{-1} for hmboH. All the CC bands are well within

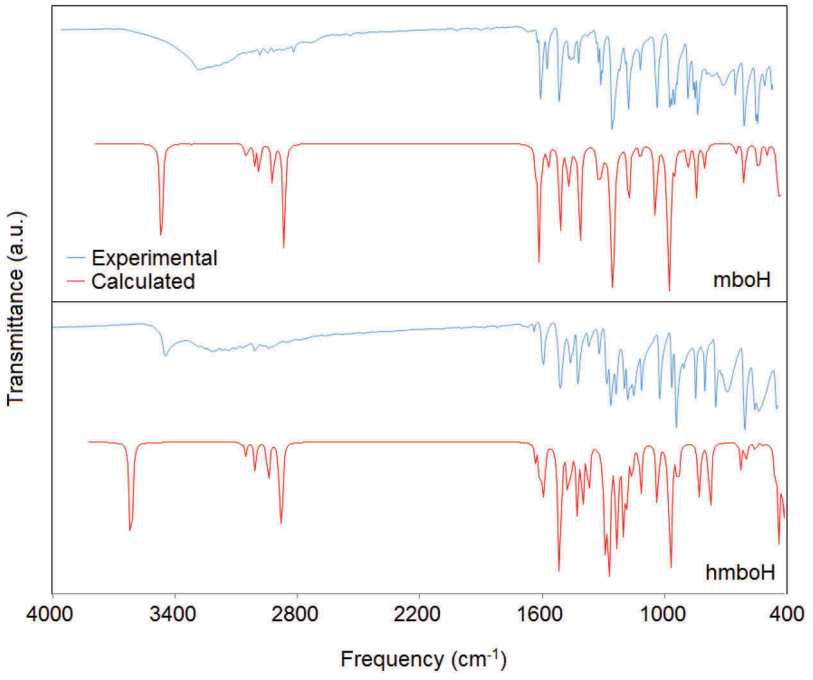

Figure 3. Experimantal (blue) and calculated (red) IR spectra of the mboH and hmboH.

the expected range [41–44]. The most characteristic band in the oxime molecules is NO stretching vibration. This vibration mode is usually independent of the rest of the modes in the molecule. The NO stretchings for both oxime molecules were observed at 964 cm^{-1} in the mboH and 948 cm^{-1} in the hmboH, as sharp bands, while these vibration modes were calculated at 967 and 971 cm^{-1}, respectively. In addition, the C-O stretching vibrations were observed at ca. 1028 cm^{-1}, while calculated at 1035 cm^{-1} for both oxime molecules. Although the calculated vibrational frequencies in some cases significantly deviate from the experiment, the correlations are very linear (r^2 = 0.9991 for mboH and r^2 = 0.9972 for hmboH) as seen in Figure S2.

3.2.2. *Uv-vis spectra*

The UV-vis. electronic spectra of mboH and hmboH have been investigated by experimental and theoretical calculation at the range of 800–200 nm in 5 × 10^{-5} M EtOH solutions and a 10 mm quartz cuvette. Time dependent density functional theory (TDDFT), allowing for the best compromise between accuracy and computational cost, has recently emerged as a great tool for examining the static and dynamic properties of the molecules in their excited states. Therefore, the absorption bands of the title compounds were assigned based on TDDFT/CAM-B3LYP in EtOH solution using the CPCM method. First 12 singlet-excited states were calculated to predict the transition energies. The calculated absorptions with oscillator strengths lower than 0.03 were not taken into consideration. The calculated and experimental absorption values are listed in Table S4, while the absorption spectra of both molecules are showed in Figure 4. The mboH and hmboH display three main absorption bands centred at 295, 265 and 215 nm for mboH and 305, 270 and 215 nm for hmboH in the experimental spectrum. The absorption coefficients (ε) were calculated as 3021.9, 2111.4 and 14574.3 $dm^3mol^{-1}cm^{-1}$ for mboH, 6773.6, 12,296.5 and 21,233.4 $dm^3mol^{-1}cm^{-1}$ for hmboH, respectively. However, the calculated spectrum shows four transitions at 266, 251, 207 and 203 nm (f_{os} = 0.5538–0.0511) in the mboH and three transitions at 283, 257 and 215 nm (f_{os} = 0.7157–0.1100) in the hmboH.

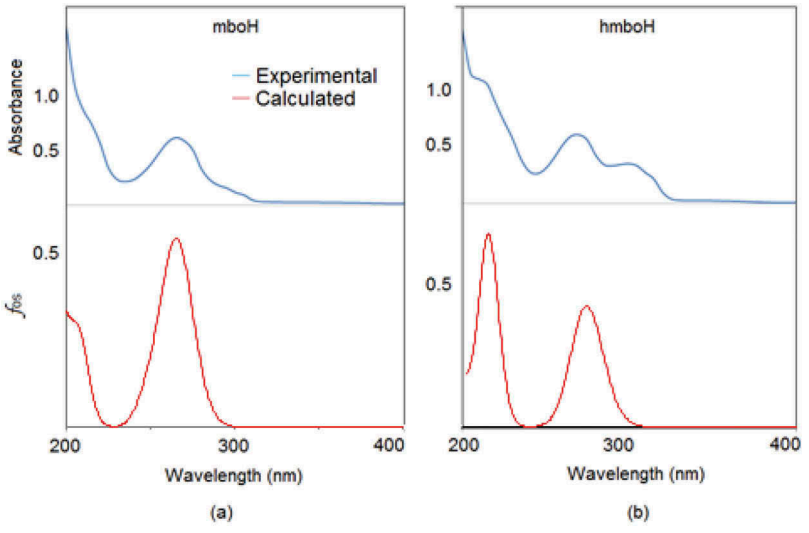

Figure 4. Experimental (blue) and calculated (red) electronic spectra of (a) mboH and (b) hmboH.

The TDDFT calculation of molecular orbital geometry shows that the highest wavelength of the both molecules resembles the electronic transition from HOMO to LUMO. This transition mode is measured to be 295 nm for mboH and 305 nm for hmboH, while calculated 266 and 283 nm, respectively. The other bands the observed in high energy region (λ_{max} = 265 and 215 nm for mboH and λ_{max} = 270 and 215 nm for hmboH) chiefly formed by two electronic transition modes HOMO → LUMO+2 and HOMO-1 → LUMO are calculated to be 251 and 207 nm for mboH, 257 and 215 nm for hmboH with the minor difference of percent. An overview of the contour plots and relative energy of occupied (HOMO) and unoccupied (LUMO) molecular orbitals help explain the assignment of the calculated orbital excitations to the experimental band. The HOMO-1 and LUMO+2 orbitals are mainly located on one of the phenyl side, while HOMO, LUMO and LUMO+3 orbitals are localised on the oxime and phenyl groups in the both molecules. All of the calculated molecular orbitals have π character. Therefore, all electronic transitions can be ascribed to the π→π* transitions for both molecules.

3.3. *Optical properties*

3.3.1. *Nonlinear optical properties (NLO)*

A good NLO material () has been frequently used in telecommunications, signal processing, optical interconnections and optical memory devices. Organic molecules able to manipulate photonic signals efficiently are of importance in technologies. Theoretical studies on electronic properties have been done in order to understand the microscopic origin of nonlinear behaviour of the different organic molecules. First hyperpolarisibility is a third rank tensor that can be described by a 3 × 3 × 3 matrix. The 27 components of the 3D-matrix can be reduced to 10 components due to the Kleinman symmetry [45]. The components of β are defined as the coefficients in the Taylor series expansion of the energy in the external electric field. When the external electric field is weak and homogeneous this expansion becomes:

$$E = E^0 - \mu_i F_i - 1/2\alpha_{ij}F_iF_j - 1/6\beta_{ijk}F_iF_jF_k + 1/24\gamma_{ijkl} \quad (1)$$

where E^0 is the energy of the unperturbed molecules, F_i the field at the origin and μ_i, α_{ij} and β_{ijk} are the components of dipole moment, polarizability, and the first hyperpolarisability,

respectively. The total static dipole moment (μ), the linear polarizability (α) and the first hyperpolarisability (β) using the x, y, z components are calculated using the following equations [46]:

$$\mu = \sqrt{\mu_x^2 + \mu_y^2 + \mu_z^2} \tag{2}$$

$$\alpha = \frac{\alpha_{xx} + \alpha_{yy} + \alpha_{zz}}{3} \tag{3}$$

$$\beta = \sqrt{(\beta_{xxx} + \beta_{xyy} + \beta_{xzz})^2 + (\beta_{yyy} + \beta_{xxy} + \beta_{yzz})^2 + (\beta_{zzz} + \beta_{xxz} + \beta_{yyz})^2} \tag{4}$$

Since the x, y, z components of α and β of Gaussian 09 output are reported in an atomic mass unit (a.u.), the calculated values have been converted into $Å^3$ and electrostatic unit (e.s.u.) using (for):1 a.u. = 0.1482 $Å^3$; for β: 1 a.u. = 0.0086393 × 10^{-30} e.s.u.). The dipole moment (μ), the linear polarisability (α) and the first hyperpolarisability (β) were calculated in vacuum at the B3LYP/6–311++G(d,p) level for the mboH and hmboH. In addition, the NLO properties were investigated using polarised continuum model (PCM) [47] with same level in different solvents which are benzene, chloroform, ethanol, dimethyl sulfoxide (DMSO) and water, and presented in Table 1.

The calculated dipole moment (μ) is 1.987 and 2.899 D in vacuum for mboH and hmboH, respectively. These values were calculated at 2.428 and 3.434 D in benzene (ε = 2.28), at 2.699 and 3.688 D in chloroform (ε = 4.81), at 2.919 and 3.985 D in etnaol (ε = 24.60). Then the rate of increase of dipole moment declined and almost stabilised for DMSO and water. These changes are better seen in Figure 5. The linear polarizability (α) for mboH and hmboH were calculated 18.067 and 18.573 $Å^3$ in vacuum, respectively. This value also increases with increasing dielectric constants in different solvents, and then fixed as similar to dipol moment values (Figure 5). The calculated first hyperpolarisibilities (β) of mboH and hmboh in vacuum are 6.102 × 10^{-30} and 6.910 × 10^{-30} e.s.u. These results indicate that the hmboH molecule possesses better NLO properties than the mboH. The high β value and μ value different from zero indicate that the both molecules might be a good candidate of NLO material and can also be considered to be an important class of compounds in medical chemistry.

3.3.2. *Energy gap between HOMO and LUMO orbitals determination of mboH and hmboH*

The UV-vis absorbance spectra of thin films (an average thickness of 1 μm) were used to determine the analysis of optical gap of mboH and hmboH using the Tauc relation, as given following equation [48].

$$\alpha h\nu \approx \left(h\nu - E_g\right)^n$$

where α is the absorption coefficient in cm^{-1}, E_g is the energy gap between HOMO and LUMO orbitals, and $h\nu$ is the photon energy. The E_g of the mboH and hmboH are obtained by extrapolation to $\alpha = 0$ when $n = 2$ for a direct allowed transition and $n = 1/2$ for an indirect allowed transition. The absorption data is fitted to the equation for direct energy gap between HOMO and LUMO orbitals transition of

Table 1. The dipole moments (μ), the linear polarizabilities (α) and the first hyperpolarizabilitis (β) in the different solvents for mboH and hmboH.

		Gas (ε = 1.00)	Benzene (ε = 2.28)	Chloroform (ε = 4.81)	Ethanol (ε = 24.60)	DMSO (ε = 47.00)	Water (ε = 78.54)
μ (D)	mboH	1.937	2.428	2.699	2.919	2.945	2.977
	hmboH	2.899	3.434	3.688	3.985	4.008	4.049
α ($Å^3$)	mboH	18.067	21.196	22.968	24.374	24.548	24.692
	hmboH	18.573	21.858	23.729	25.239	25.420	25.596
β (×10^{-30} e.s.u.)	mboH	6.102	9.322	11.733	13.953	14.283	14.477
	hmboH	6.910	10.839	13.852	16.871	17.067	17.726

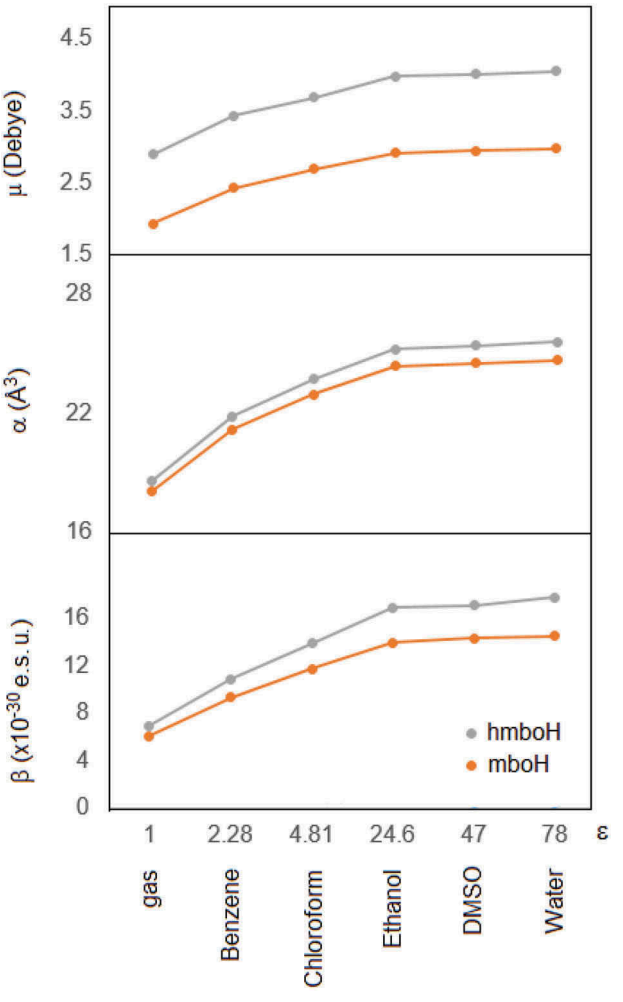

Figure 5. The change of the dipole moments (μ), the linear polarizabilities (α) and the first hyperpolarizabilitis (β) in the different solvents for mboH and hmboH.

mboH and hmboH. Figure 6 shows $(\alpha h\nu)^2$ versus $h\nu$ for a direct allowed transition. As shown in Figure 6 and Table S6, the mboH and hmboH show a perfect fit and the extrapolation yielding E_g values of 4.326 and 4.282 eV, respectively for direct allowed transition. The theoretical energy gap between HOMO and LUMO orbitals values of mboH and hmboH were calculated as 4.733 and 4.542 eV, respectively with B3LYP/6–311++G(d,p) level.

3.4. *Physicochemical properties*

Some physicochemical properties, such as Mulliken and NBO charges (Table S5 and Figure S3), FMOs (Table S6 and Figure S4), MEP (Figure S5) and thermodynamic properties (Table S7 and Figure S6) were discussed in supplementary materials [49–56].

3.4.1. *Fukui function indices*

Fukui function plays the important role in determining whether the molecule will accept or donate electrons which are more prone to undergo a nucleophilic or an electrophilic attack,

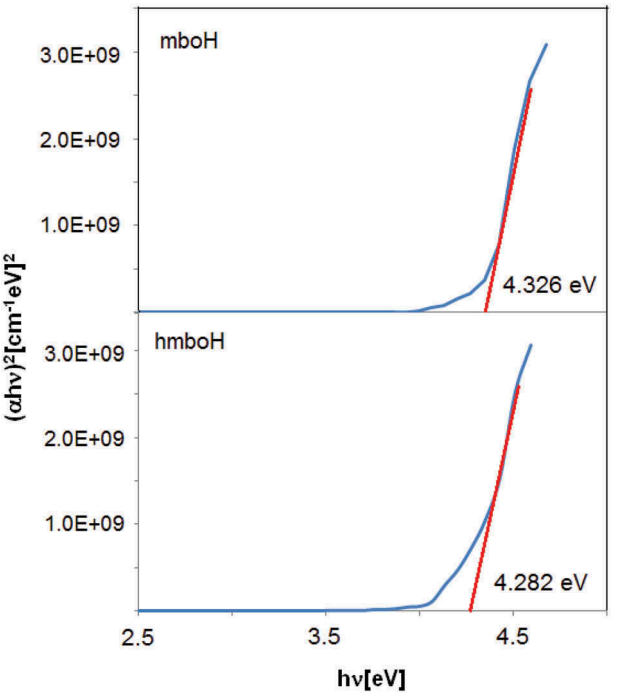

Figure 6. Plot of $(\alpha h\nu)^2$ versus $h\nu$ for direct allowed transition of mboH and hmboH (α, absorption coefficient is calculated from A/d formula, A and d are absorbance and thickness, respectively).

respectively. Partial atomic charges and atomic Fukui function indices are good indicators of selectivity, that is, the region on the molecule on which certain type of reactions is likely to occur. The regions of a molecule where the Fukui function is large are chemically softer than the regions where the Fukui function is small. The atomic Fukui functions calculated from the Mulliken or NBO atomic charges, but the NBO charges give better results than Mulliken charges [57]. The Fukui function indices have been calculated by taking the finite difference approximations in both oxime molecules:

$$f^{+} = \left(q_{N+1} - q_N\right)$$

$$f^{-} = \left(q_N - q_{N-1}\right)$$

Here 'q' is the natural charge of atom in the molecule, that is, the electron density at a point in space around the molecule. The 'N' corresponds to the number of electrons in the neutral molecule. 'N + 1' corresponds to an anion, 'N-1' corresponds to a cation, with an electron removed from the HOMO of the neutral molecule.

The values performed at the ground state geometry based on NBO charges are listed in Table 2. It has been found that the highest f–value which preferred site for electrophilic attack is the atom in the molecule is −0.126 in the mboH and −0.115 in the hmboH. From Table 2 indicates that the reactivity order for the electrophilic case as O2 > C1> O1> N1> C4> C3> C5> C2> C6> C7> C8 for mboH and O2≅ C1> O1> C4> N1> C3≅ C6> O3> C5> C7> C2> C8 for hmboH. Reactivity of similar atoms of different molecules can also be compared by calculating condensed softness indices from the Fukui function indices and global softness (S) by using the following equations [58]:

$s^{+} = f^{+} . S$

$s^{-} = f^{-} . S$

Table 2. Condensed Fukui function and local softness indices for the both oximes.

Atom	q_{N-1}	q_N	q_{N+1}	f^+	f^-	s^+	s^-
mboH							
C1	−0.011	−0.134	−0.152	−0.018	−0.123	−0.004	−0.027
C2	−0.116	−0.157	−0.185	−0.028	−0.041	−0.006	−0.009
C3	−0.229	−0.293	−0.310	−0.017	−0.064	−0.004	−0.014
C4	0.421	0.335	0.266	−0.069	−0.086	−0.015	−0.019
C5	−0.178	−0.229	−0.236	−0.007	−0.051	−0.001	−0.011
C6	−0.131	−0.148	−0.211	−0.063	−0.017	−0.013	−0.004
C7	0.043	0.033	−0.051	−0.084	−0.010	−0.018	−0.002
C8	−0.227	−0.206	−0.230	−0.024	0.021	−0.005	0.005
N1	−0.002	−0.111	−0.208	−0.097	−0.109	−0.021	−0.024
O1	−0.403	−0.523	−0.570	−0.047	−0.120	−0.010	−0.026
O2	−0.410	−0.536	−0.561	−0.025	**−0.126**	−0.005	**−0.028**
hmboH							
C1	−0.002	−0.117	−0.131	−0.014	−0.115	−0.003	−0.025
C2	−0.255	−0.252	−0.273	−0.021	0.003	−0.004	0.001
C3	0.333	0.259	0.252	−0.007	−0.074	−0.001	−0.016
C4	0.397	0.295	0.236	−0.059	−0.102	−0.013	−0.022
C5	−0.213	−0.233	−0.242	−0.009	−0.020	−0.002	−0.004
C6	−0.095	−0.169	−0.221	−0.052	−0.074	−0.011	−0.016
C7	0.038	0.033	−0.044	−0.077	−0.005	−0.016	−0.001
C8	−0.216	−0.201	−0.230	−0.029	0.015	−0.006	0.003
N1	−0.010	−0.108	−0.195	−0.087	−0.098	−0.019	−0.022
O1	−0.417	−0.522	−0.564	−0.042	−0.105	−0.009	−0.023
O2	−0.552	−0.667	−0.696	−0.029	**−0.115**	−0.006	**−0.025**
O3	−0.501	−0.570	−0.586	−0.016	−0.069	−0.003	−0.015

These equations envisage the most electrophilic site in a molecule has maximum value of s^+ while maximum value of s^- corresponds to the nucleophilic site in the molecule. The local reactivity descriptors, $s^{\pm}$ provides the reactivity tendencies of local site during nucleophilic or electrophilic attacks. MEPs counter and Fukui function analysis demonstrate that the O2, C1, O1, N1 and C4 atoms are reactive atoms for electrophilic attack. The both oxime molecules are more electrophilic attack than nucleophilic attack. These results show mboH and hmboH molecules act as more biological activity.

3.4.2. *NBO analysis*

The NBO calculations were performed using DFT/B3LYP method and 6–311++G(d,p) basis set with Pop = NBO keyword in order to understand various second-order interactions between the filled orbital of one subsystem and vacant orbital of another subsystem, which is a measure of the intra-molecular delocalisation or hyper conjugation. The second order Fock matrix was carried out to evaluate the donor-acceptor interactions in the NBO calculation. For each donor (i) and acceptor (j), the stabilisation energy ($E2$) associates with electron delocalisation between i and j is estimated as [59]

$$E(2) = -qi\left(Fij^2/\varepsilon j - \varepsilon i\right)$$

where qi is the donor orbital occupancy, εj and εi large diagonal elements, Fij is the off diagonal NBO Fock matrix element. The corresponding results are presented in Table 3.

In the NBO analysis, large $E(2)$ value shows the intensive interaction between electron-donors and electron-acceptors, and the greater the extent of conjugation of the whole system. A different level of π electron delocalisation is observed between C1 = C2, C3 = C4 and C5 = C6 in the both molecules. The strongest interaction between the lone pair LPO2 with that of antibonding C4-C5, with stabilisation energies 128.49 and 116.48 kJ/mol, respectively for mboH and hmboH, denotes larger delocalisation within the phenyl ring system. In addition, a contribution for the molecular stabilisation of hmboH is further given by the intramolecular interaction formed by the orbital

overlap between LPO3 and O2-H antibonding orbital, with stabilisation energy 6.49 kJ/mol, which is a consequence of hyperconjugation between methoxy oxygen lone pair electron pairs and hydroxyl σ* antibonding orbitals, resulting in the formation of intramolecular O-H·····O hydrogen bond.

In the case of LP (1) of nitrogen atom (N1) to the antibonding acceptor σ* (O1-H) in the mboH and σ* (N1-O1) in the hmboH, there is a low stabilisation energy of 2.38 kJ/mol for both molecules shown in Table 3.

3.5. *Molecular docking studies*

3.5.1 *DNA binding studies*

The molecular docking studies were conducted in order to validate the obtained biological and pharmacological data and to provide understandable evidence for the observed anticancer and antimicrobial activity of mboH and hmboH molecules. Recently, the well establishes techniques to calculate the interaction of two molecules such as DNA and ligand or protein and ligand are presented in the literature. These techniques find the best orientation of ligand that would form a complex with overall minimum energy. Therefore, the theoretical calculations of the interactions with DNA and HSA are significant, and these interactions were studied in this and next sections. It was built to discussion the binding modes using Autodock/Vina program.

In order to obtained the binding site, blind docking was performing on the DNA dodecamer with a d(CGCGAATTCGCG) sequence (PDB ID: 1BNA). The grid map was set to 60 × 60 × 60 $Å^3$ along the x, y and z axes with 0.375 Å grid spacing. The centre of the grid map was set to 14.779, 20.976 and 8.804 Å. The conformations were ranked based on the lowest free binding energy. The results of the docking revealed that the mboH and hmboH molecules interactions with the DNA minor grove, which is C-G rich region, as seen Figure 7. In the mboH, there are hydrophobic interactions between the mboH molecule atoms and based of DNA, viz., DC9, DG10, DC11 and DG16, while the interactions of hmboH with DNA (DC9, DC11 and DG16) are weak hydrogen bonds and hydrophobic interactions. The binding free energies of mboH and hmboH were calculated to be −23.012 and −25.522 k*J*mol^{-1}, respectively. The binding free energies indicate a high binding affinity between the oxime molecules with DNA, and the affinity of hmboH molecule is higher than that of the mboH molecule.

3.5.2. *Docking with protein*

Molecular docking is playing an increasingly important role in drug design for the treatment of many diseases. The graphical user interface program 'Autodock Tools' was used to prepare and analyse the docking simulations and running Autodock/Vina program. This docking software design as an automated to predict how our molecules may be drug candidates bind to a receptor.

The mboH and hmboH were selected to be docked into the active site of protein (PDB ID: 5FCT) which belongs to the class of proteins exhibiting the property as a Dihydrofolate synthase inhibitor. The ligands were docked into the functional sites of the respective protein individually and the docking energies were examined to achieve a minimum value. Autodock/Vina result indicates the binding position and bound conformation of the mboH and hmboH, together with a rough estimate of its interaction. Docked conformation, which calculated the lowest binding energy, was chosen to investigate the mode of binding. The dominating configurations of the mboH-protein and hmboH-protein complexes are showed in Figure 8. The binding free energies of the mboH and hmboH with protein were computed to be −26.359 and −25.941 k*J* mol^{-1}, respectively. Molecular docking study revealed that the most stable conformers of the mboH and hmboH are surrounded by the residues (within 3.5 Å) ASN, HIS, PHE, GLU, ASN (Figure 8).

Table 3. Second order perturbation theory analysis of Fock matrix in NBO basis for mboH and hmboH.

Donor (*i*)	Type	ED/e	Acceptor (*j*)	Type	ED/e	E(2)[a] (kJ/mol)	E(j)-E(i)[b] (a.u.)	F(i,j)[c] (a.u.)
mboH								
C5-C6	π	1.71507	C3-C4	π*	0.38524	91.17	0.28	0.071
			C1-C2	π*	0.37797	70.46	0.29	0.063
C3-C4	σ	1.97805	C4-C5	σ*	0.02346	16.57	1.27	0.063
C3-C4	π	1.66413	C5-C6	π*	0.27406	62.89	0.30	0.061
			C1-C2	π*	0.37797	92.59	0.30	0.073
C2-C3	σ	1.97424	C4-O2	σ*	0.03022	19.37	1.06	0.063
C1-C2	σ	1.97451	C2-C3	σ*	0.01297	11.76	1.27	0.054
			C1-C6	σ*	0.02580	16.02	1.26	0.062
C1-C2	π	1.66249	C5C6	π*	0.27406	82.63	0.29	0.068
			C3-C4	π*	0.38524	72.34	0.27	0.062
			C7-N1	π*	0.18128	82.63	0.27	0.068
C1-C6	σ	1.97168	C1-C2	σ*	0.02104	16.19	1.26	0.063
C1-C7	σ	1.96999	N1-O1	σ*	0.01855	20.00	0.94	0.060
C7-N1	π	1.95474	C1-C2	π*	0.37797	34.89	0.36	0.054
LPO1	π	1.99228	C7-N1	π*	0.18128	88.16	0.35	0.078
LPO2	σ	1.96337	C4-C5	σ*	0.02346	3.14	1.10	0.026
			C3-C4	σ*	0.02914	28.70	1.11	0.078
			C8-H	σ*	0.00892	12.05	0.94	0.047
			C8-H	σ*	0.01866	3.18	0.92	0.024
LPO2	π	1.83692	C4-C5	π*	0.27406	128.49	0.34	0.097
			C8-H	σ*	0.01866	23.18	0.69	0.057
LPN1	σ	1.94815	C1-C7	σ*	0.02505	5.90	0.89	0.032
			C7-H	σ*	0.03424	38.33	0.79	0.076
			O1-H	σ*	0.00566	2.38	0.68	0.018
hmboH								
C4-C5	σ	1.97442	C3-C4	σ*	0.03647	15.40	1.25	0.061
C4-C5	π	1.64267	C2-C3	π*	0.39581	82.84	0.28	0.067
			C1-C6	π*	0.39782	90.29	0.3	0.072
C5-C6	σ	1.97532	C4-O2	σ*	0.01974	16.99	1.06	0.058
C3-C4	σ	1.97081	C4-C5	σ*	0.0218	15.77	1.28	0.062
			C2-C3	σ*	0.02383	17.57	1.28	0.066
C2-C3	σ	1.97637	C3-C4	σ*	0.03647	18.24	1.26	0.066
C2-C3	π	1.71276	C4-C5	π*	0.38533	75.40	0.3	0.067
			C1-C6	π*	0.39782	71.30	0.31	0.067
C1-C2	σ	1.96980	C1-O3	σ*	0.02833	20.54	1.03	0.064
			C1-C6	σ*	0.02463	15.86	1.27	0.062
C1-C6	σ	1.97189	C1-C2	σ*	0.02014	16.11	1.25	0.062
C1-C6	π	1.64215	C4-C5	π*	0.38533	83.09	0.27	0.066
			C2-C3	π*	0.39581	86.19	0.26	0.066
			C7-N1	π*	0.18192	69.50	0.26	0.062
C1-C7	σ	1.96997	N1-O1	σ*	0.01834	19.83	0.94	0.06
C7-N1	π	1.99076	C1-C6	π*	0.39782	30.88	0.37	0.051
LPO3	σ	1.96017	C3-C4	σ*	0.03647	4.52	1.11	0.031
			C2-C3	σ*	0.02383	27.61	1.14	0.078
			C8-H	σ*	0.00852	11.30	0.95	0.046
			C8-H	σ*	0.01817	2.85	0.93	0.023
			O2-H	σ*	0.01233	6.49	0.98	0.035
LPO3	π	1.86321	C2-C3	π*	0.39581	108.62	0.35	0.091
			C8-H	σ*	0.00852	22.64	0.7	0.057
			C8-H	σ*	0.01817	22.59	0.7	0.057
LPO2	σ	1.97764	C3-C4	σ*	0.03647	23.39	1.15	0.072
LPO2	π	1.86640	C4-C5	π*	0.38533	116.48	0.35	0.094
LPN1	σ	1.94761	C1-C7	σ*	0.02481	5.90	0.89	0.032
	σ		C7-H	σ*	0.03448	38.58	0.79	0.077
	σ		N1-O1	σ*	0.01834	2.38	0.68	0.018
	σ		O1-H	σ*	0.00565	4.35	0.82	0.026
LPO1	π	1.89390	C7-N1	π*	0.18192	88.28	0.35	0.078

[a]E(2) means energy of hyper-conjugative interactions (stabilisation energy).
[b]Energy difference between donor and acceptor i and j NBO orbitals.
[c]F(i,j) is the Fock matrix element between i and j NBO orbitals.

Figure 7. Computational docking models (using the Autodock/Vina software) illustrating the interactions between DNA (PDB code: 1BNA) and mboH, hmboH.

4. Conclusion

In this work, two oxime molecules, namely 4-methoxy-benzaldehyde oxime (mboH) and 4-hydroxy-3-methoxy-benzaldehyde oxime (hmboH) have been synthesised and characterised by IR and elemental analysis. After then, the DFT/B3LYP theory has been successfully employed using 6–311++G(d,p) basis set for mboH and hmboH to support the experimental findings and to evaluate some important parameters, bond length, bond angle, frequency, Mulliken and NBO charge distributions, Fukui function indices, HOMO-LUMO energy gap (ΔE), MEP, chemical reactivity, NLO properties, thermodynamic properties etc. In general, a good agreement mboH and hmboH experimental and theoretical normal modes of vibrations has been investigated.

In order to study electronic properties of both molecules, the theoretical calculations were successfully performed by using TDDFT method. The calculated data were in agreement with the observed data. All electronic transitions of both molecules can be $\pi \rightarrow \pi^*$ transition. The nonlinear optical properties were also investigated with same level in different solvents which are benzene, chloroform, ethanol, dimethyl sulfoxide (DMSO) and water. The calculated first hyperpolarisibilities (β) of mboH and hmboH in vacuum are 6.102×10^{-30} and 6.910×10^{-30} e.s.u. The β values of mboH and hmboH are about 16.4 and 18.5 times more than that of standard NLO material urea. These results indicate that the both compounds might be a good candidate of NLO material and can also be considered to be an important class of compound inmedical chemistry because if theirs high electrophilicity indexes (2.978 for mboH and 2.991 for hmboH). The various types of intramolecular electron interactions and their stabilisation energies were determined by NBO analysis. The analysis reveals large electron delocalisation within the phenyl ring system. The predicted MEP figure revealed the negative and positive regions of the molecules. Thermodynamic parameters, C, S and H increases as the temperature increases which is attributed

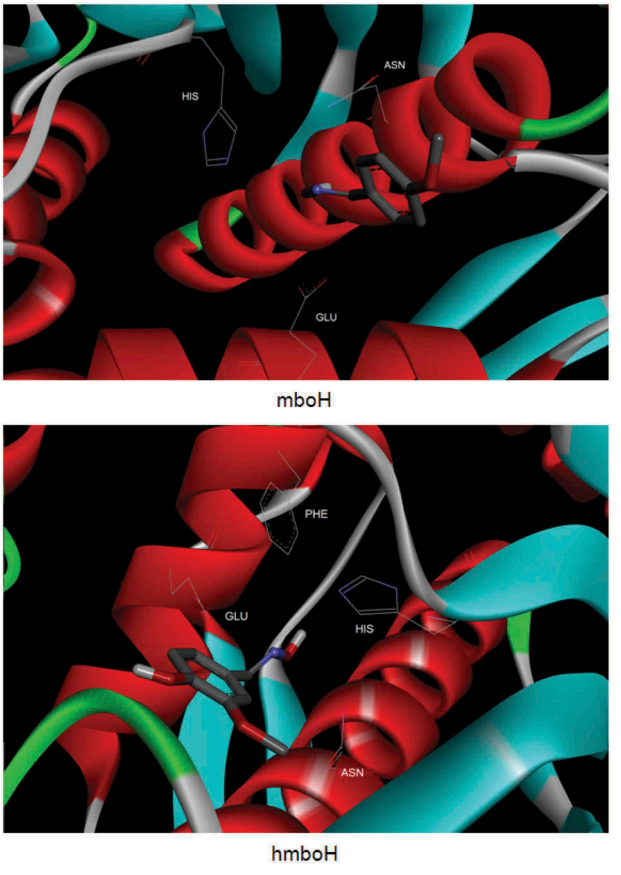

Figure 8. Docking snapshot of mboH and hmboH with protein receptor (PDB code: 5FCT).

to the enhancement of the molecular vibration. In the binding process, the binding free energies of DNA docking of mboH and hmboH were calculated at −23.012 and −25.522 k*J*mol^{-1}, respectively. Binding of the both molecules to DNA through minor groove was determined by molecular docking studies. The mboH and hmboH were selected to be docked into the active site of the protein 5FCT which belongs to the class of proteins exhibiting the property as a Dihydrofolate syntase (DHFS) inhibitor and had a minimum binding energies of −26.359 and −25.941 k*J*mol^{-1}, respectively.

Disclosure statement

No potential conflict of interest was reported by the authors.

References

[1] Kolandaivel P, Senthilkumar K. Ab initio and DFT studies on structure and stability of aliphatic aldoxime molecules. J Mol Struct (Theochem). 2001;535:61.
[2] Bekhradnia AR, Arshadi S. Conformational analysis, infrared, and florescence spectra of 1-Phenyl-1,2-Propandione-1-Oxime and related tautomers: experimental and theoretical study. Monatshefte für Chemie. 2007;138:725.
[3] Afonin AV, Ushakov IA, Pavlov DV, et al. Study of conformations and hydrogen bonds in the configurational isomers of pyrrole-2-carbaldehyde oxime by 1H, 13C and 15N NMR spectroscopy combined with MP2 and DFT calculations and NBO analysis. Magn Reson Chem. 2010;48:685.

[4] Jayabharathi J, Manimekalai A, Padmavathy M. Syhthesis, spectral, theoretical and antimicrobial of some heterocyclic oximes. Med Chem Res. 2011;20:981.
[5] Kaya Y, Yilmaz VT, Arslan T, et al. Experimental and theoretical DFT studies of structure, spectroscopic and fluorescence properties of a new imine oxime derivative. J Mol Struc. 2012;1024:65.
[6] Chakravorty A. Structural chemistry of transition metal complexes of oximes. Coord Chem Rev. 1974;13:1.
[7] Chaudhuri P. Homo- and hetero-polymetallic exchange coupled metal-oximates. Coord Chem Rev. 2003;243:143.
[8] Milios CJ, Stamatatos TC, Perlepes SP. The coordination chemistry of pyridyl oximes. Polyhedron. 2006;25:134.
[9] Nakamura H, Iitaka Y, Sakakibara H, et al. The molecular and crystal structure determination of bisanhydroalthiomycin by the x-ray diffraction method. J Antibiot. 1974;27:894.
[10] Kirst HA, Szymanski EF, Doman DE, et al. Structure of althiomycin. J Antibiot. 1975;28:286.
[11] Ponomareva VV, Halley NK, Kou X, et al. Synthesis, spectra and crystal structures of complexes of ambidentate C 6 H 5 C (O) C (NO) CN–J. Chem Soc Dalton Trans. 1996;2351.
[12] Hambley TW, Ling ECH, O'Mara S, et al. Increased targeting of adenine-rich sequences by (2-amino-2-methyl-3-butanone oxime)dichloroplatinum(II) and investigations into its low cytotoxicity. J Biol Inorg Chem. 2000;5:675.
[13] Quiroga AG, Cubo L, de Blas E, et al. Trans platinum complexes design: one novel water soluble oxime derivative that contains aliphatic amines in trans configuration. Inorg Biochem. 2007;101:104.
[14] Zorbas-Seifried S, Jakupec MA, Kukushkin NV, et al. Reversion of structure-activity relationships of antitumor platinum complexes by acetoxime but not hydroxylamine ligands. Mol Pharmacol. 2007;71:357.
[15] Scaffidi-Domianello Y, Yu Meelich K, Jakupec MA, et al. Novel *cis*- and *trans*-configured bis(oxime) platinum(II) complexes: synthesis, characterization, and cytotoxic activity. Inorg Chem. 2010;49:5669.
[16] Lipkowitz KB, Boyd D, editors. Reviews in computational chemistry. Vol. 13. New York (NY): Wiley-VCH; 1999.426p.
[17] Nagy PI, Kokosi J, Gergely A, et al. Theoretical conformational analysis for codeinone-6-oximes in gas phase and in solution. J Phys Chem A. 2003;107:7861.
[18] Georgieva I, Trendafilova N. Comprehensive DFT and MO studies on glyoxilic acid oxime and related ions in gas phase and solution: conformations, basicities and acidities. Chem Phys. 2006;321:311.
[19] Sharma K, Mishra SB, Mishra AK. Synthesis and mechanistic study of steroidal oxime ethers. Helv Chim Acta. 2011;94:2256.
[20] Guimaraes AP, Franca TCC, Ramalho TC, et al. Docking studies and effects of. syn-anti isomery of oximes derived from pyridine. imidazol bicycled systems as potential human. acetylcholinesterase reactivators. J Appl Biomed. 2011;9:163.
[21] Malek K, Vala M, Kozlowski H, et al. Experimental and theoretical NMR study of selected oxocarboxylic acid oximes. Magn Reson Chem. 2004;42:23.
[22] Golec B, Mielke Z. Formaldoxime dimers: infrared matrix isolation and theoretical study. J Mol Struct. 2007;844–845:242.
[23] Golec B, Grzegorzek J, Mielke Z. Complexation of formaldoxime and acetaldoxime with nitrogen. Chem Phys. 2008;353:13.
[24] Irshaidat T. Some physical organic aspects of salicylaldehydes oximes, a theoretical study. Tetrahedron Lett. 2008;49:631.
[25] Istomina NV, Shcherbina NA, Krivdin LB. ^{13}C-^{13}C spin-spin coupling constants in structural studies: XLIV. Carbonyl-containing oximes. Russ J Org Chem. 2009;45:481.
[26] Arjunan V, Mythili CV, Mageswari K, et al. Experimental and theoretical investigations of benzamide oxime. Spectrochim Acta Part A. 2011;79:245.
[27] Gonewar NR, Jadhav VB, Jadhav KD, et al. Theoretical calculations of infrared, NMR and electronic spectra of 2-nitroso-1, naphthol or 1-2 naphthoquinine-2 oxime and comparison with experimental data. Res Pharm. 2012;2:18.
[28] Schwarz L, Girreser U, Clement B. Synthesis and characterization of *para*-Substituted *N, N'*-Dihydroxybenzamidines and their derivatives as model compounds for a class of prodrugs. Eur J Org Chem. 2014;9:1961–1975.
[29] Frisch MJ, Trucks GW, Schlegel HB, et al. Gaussian 09, revision C.01. Wallingford (CT): Gaussian, Inc; 2010.
[30] Grimme S, Antony J, Ehrlich S, et al. A consistent and accurate ab initio parametrization of density functional dispersion correction (DFT-D) for the 94 elements H-Pu J. Phys Chem. 2010;132:154104.
[31] Becke AD. Density-functional thermochemistry. III. The role of exact exchange. J Chem Phys. 1993;98:5648.
[32] Sundaraganesan N, Ilakiamani S, Saleem H, et al. FT-Raman and FT-IR spectra, vibrational assignments and density functional studies of 5-bromo-2-nitropyridine. Spectrochim Acta A. 2005;61:2995.
[33] Jesus AJL, Rosado MTS, Reva I, et al. Structure of isolated 1,4-Butanediol: combination of MP2 calculations, NBO analysis, and matrix-isolation infrared spectroscopy. J Phys Chem A. 2006;110:4669.
[34] Dennington R, Keith T, Millam J, et al. GaussView, version 3.07. ShawneeMission (KS): SemichemInc; 2003.
[35] Pearson RG. The electronic chemical potential and chemical hardness. J Mol Struc-Theochem. 1992;255:261.

[36] Parr RG, Szentpaly L, Liu S. Electrophilicity index. J Amer Chem Soc. 1999;121:1922.
[37] Trott O, Olson AJ. AutoDock Vina: improving the speed and accuracy of docking with a new scoring function, efficient optimization, and multithreading. J Comput Chem. 2010;31:455.
[38] Boopathi M, Udhayakala P, Ramkumaar GR, et al. Microwave assisted synthesis of some 5-substituted imidazolone analogs as a new class of non purine xanthine oxidase inhibitors. Der Pharma Chemica. 2015;7:110.
[39] Kaya Y, Icsel C, Yilmaz VT, et al. Palladium(II) and platinum(II) complexes of a new imineoxime ligand – structural, spectroscopic and DFT/time-dependent (TD) DFT studies. J Organometal Chem. 2014;752:83.
[40] Alver O, Kaya MF, Bilge M, et al. Vibrational spectroscopic investigation and conformational analysis of methacrylamidoantipyrine: a comparative density functional study. J Theor Chem. 2013;2013:10.
[41] Castro ME, Percino MJ, Chapela VM, et al. Theoretical and experimental spectroscopic analysis of cyano-substituted styrylpyridine compounds. Int J Mol Sci. 2013;14:4005.
[42] Li Y, Liu YY, Chen XJ, et al. Synthesis, spectroscopic characterization, X-Ray structure, and DFT calculations of some new 1,4-Dihydro-2,6-Dimethyl-3,5 -Pyridinedicarboxamides. Plos one. 2014;9:1.
[43] Singh HJ, Sirivastava P. Computational studies on the structure and vibrational spectra of 2-hydroxy-5-methyl-3-nitropyridine. Ind J Pure Appl Phys. 2009;47:557.
[44] Kucuk I, Kaya Y, Kaya AA. Structural, spectroscopic (FT-IR, NMR, UVevisible), nonlinear optical (NLO), cytotoxic and molecular docking studies of 4-nitroisonitrosoacetophenone (ninapH) by DFT method. J Mol Strc. 2017;1139:308.
[45] Kuleshova LN, Antipin MY, Khrustalev VN, et al. Polymorphism and design of noncentrosymmetric crystals of 4-Hydroxybenzaldehyde-4-Nitrophenylhydrazone and N'-(2-Phenyl-1H-Indole-3-Aldehyde)-4-Nitrophenylhydrazone. Kristallografiya. 2003;48:594.
[46] Albayrak C, Odabasoglu M, Ozek A, et al. Synthesis, spectroscopic characterizations and quantum chemical computational studies of (Z)-4-[(E)-(4-fluorophenyl)diazenyl]-6-[(3-hydroxypropylamino)methylene]-2-methoxycyclohexa-2,4-dienone. Spectrochim Acta Part A. 2012;85:85.
[47] Barone V, Cossi M, Thomasi J. Geometry optimization of molecular structures in solution by the polarizable continuum model. J Comput Chem. 1998;19:404.
[48] Tauc J, Grigorovici R, Vancu A. Optical properties and electronic structure of amorphous germanium. Phys Status Solidi. 1966;15:627.
[49] Subramanian N, Sundaraganesan N, Jayabharathi J. Molecular structure, spectroscopic (FT-IR, FT-Raman, NMR, UV) studies and first-order molecular hyperpolarizabilities of 1,2-bis(3-methoxy-4-hydroxybenzylidene)hydrazine by density functional method. Spectrochim Acta A. 2010;76:259.
[50] Muthu S, Renuga S. Vibrational spectra and normal coordinate analysis of 2-hydroxy-3-(2-methoxyphenoxy) propyl carbamate. Spectrochim Acta. 2014;132:313.
[51] Ternavisk RR, Camargo AJ, Machado FBC, et al. Synthesis, characterization, and computational study of a new dimethoxy-chalcone. J Mol Model. 2014;20:2526.
[52] Murray JS, Sen K. Molecular electrostatic potentials, concepts and applications. Amsterdam, The Netherlands: Elsevier; 1991.
[53] Luque EJ, Lopez JM, Orozco M. Perspective on "Electrostatic interactions of a solute with a continuum. A direct utilization of ab initio molecular potentials for the prevision of solvent ects". Theor Chem Accounts. 2000;103:343.
[54] Raja M, Muhamed RR, Muthu S, et al. Synthesis, spectroscopic (FT-IR, FT-Raman, NMR, UV–visible), first order hyperpolarizability, NBO and molecular docking study of (E)-1-(4-bromobenzylidene) semicarbazide. J Mol Struct. 2017;1128:481.
[55] Bopp F, Meixner J, Kestin J. Thermodynamics and statistical mechanics. 5th ed. New York (NY): Academic Press Inc; 1967.
[56] Ott JB, Goates JB. Chemical thermodynamics: principles and applications. San Diego: Academic Press; 2000.
[57] Nazari F, Zali FR. Density functional study of the relative reactivity of the carbonyl group in substituted cyclohexanone. J Mol Struct (Theochem). 2007;817:11.
[58] Ebenso EE, Isabirye DA, Eddy NO. Adsorption and quantum chemical studies on the inhibition potentials of some thiosemicarbazides for the corrosion of mild steel in acidic medium. Intr J Mol Scienc. 2010;11:2473.
[59] Szafram M, Komasa A, Adamska EB. Crystal and molecular structure of 4-carboxypiperidinium chloride (4-piperidinecarboxylic acid hydrochloride). J Mol Struct. 2007;827:101.